Ultrasound-Assisted Electrodeposition Synthesis of nZVI-Pd/AC Toward Reductive Degradation of Methylene Blue

Yingtao Long
Chongqing Municipal design and research insitute Co.,Ltd
Jianjun Liang (liangjianjun98@126.com)
Key Laboratory of the Three Gorges Reservoir Region's Eco-Environment (Ministry of Education),Chongqing University https://orcid.org/0000-0003-0925-7024
Yinghao Xue
Key Laboratory of the Three Gorges Reservoir Region's Eco-Environment (Ministry of Education), Chongqing University

Research Article

Keywords: Ultrasound-assisted electrodeposition, nZVI/Pd nanoparticles, activated carbon, reductive degradation.

Posted Date: May 4th, 2021

DOI: https://doi.org/10.21203/rs.3.rs-401732/v1

Version of Record: A version of this preprint was published at Environmental Science and Pollution Research on July 9th, 2021. See the published version at https://doi.org/10.1007/s11356-021-15316-0.

Abstract

A novel composite (nZVI/Pd-AC) was prepared by loading nanoscale zero-valent iron (nZVI) and Pd on activated carbon (AC) electrode under electrodeposition with ultrasound, which was used to conduct reductive degradation of methylene blue (MB). The loading contents of Fe and Pd were 15.84% and 2.06%, respectively. XPS results further confirmed that the resulting material contained Fe^0 and Pd^0. Without external conditions, MB could be degraded on the surface of nZVI/Pd-AC and reach equilibrium within 180 min. To investigate the regeneration property, re-electrodeposition strategy was effective to refresh the active sites of nZVI/Pd-AC, and the removal efficiency only reduced by 4.51% in five circles indicating the good reusability of nZVI/Pd-AC composites. GC-MS was used to identify a possible degradation pathways of MB, the results showed that the degradation products were mainly N, N-dimethylaniline and 2-amino-5-dimethylamino-benzenesulfonic acid. And the S-C, C-N bonds are the sites easier to be attacked.

Highlights

- nZVI-Pd/AC is prepared by electrodeposition.
- The degradation of methylene blue dye by nZVI-Pd/AC is satisfactory.
- Remarkable performance and reusability were shown in the degradation of dyes under the influence of various factors.
- Fe^0 reduction with enhancement of Pd catalysis play key roles in adsorption process.

1 Introduction

Dyes are widely used in the textile, paper and food packaging industries due to their low cost and long-lasting and effective dyeing properties (Zhao et al. 2015). At the same time, they have also produced massive dyeing wastewater. Dyestuffs and additives are the main pollutants in dyeing wastewater, and their high chroma and high chemical oxygen demand (COD) are the main factors harming the environment. Most dyes have complex aromatic structures and are highly resistant to microorganisms, increasing the difficulty of conventional biological wastewater treatment (Katheresan et al. 2018). In addition, physical methods such as adsorption (Xue et al. 2019) and membrane filtration (Rajeswari et al. 2019) only transfer dyes from one medium to another. Chemical coagulation/flocculation (Verma et al. 2012), advanced oxidation(Yang et al. 2015)and other methods to remove dye wastewater require high operating costs or may produce intermediate products, which are also toxic to the environment. In recent years, due to the high surface energy and reactivity, nanoscale zero valent iron (nZVI, Fe^0) has received extensive attention(Yan et al. 2013).

It has been proven in the literature that nZVI is an effective material used to remediation of groundwater and surface water contaminated by chlorinated organic (Wang et al. 2015b), heavy metals (Li et al. 2017b), nitroaromatic compounds (Zhang et al. 2009), nitrates (Chen et al. 2005) and dyes (Satapanajaru

et al. 2011, Wang et al. 2015c). However, van der Waals force and the intrinsic ferromagnetism can cause the aggregation of Fe^0 nanoparticles, reducing their mobility and chemical reactivity (Berge &Ramsburg 2009). Generally, hydrophilic or amphoteric substances as surfactants (Tian et al. 2018) and starch (Fu et al. 2015) are added to the surface of Fe^0 particles, and the aggregation of Fe^0 particles is inhibited by steric hindrance or electrostatic effect to increase the migration rate of nZVI particles in porous media. It's alternative to use polymer electrolytes to modify the surface reactivity of Fe^0 nanoparticles, such as carboxymethyl cellulose (CMC) (He &Zhao 2007) and polyacrylamide (Liu et al. 2016). The high energy can also be transferred to the reaction medium by ultrasound. By acting as a crystal growth inhibitor, the growth kinetics and the degree of aggregation of the particles can be reduced, which can lead to reduced crystallinity, cluster rupture, and smaller particle size. A certain material can also be used as a carrier to uniformly and stably support nZVI on the surface, forming a composite. Common carriers include activated carbon (Qian et al. 2017, Wu et al. 2016), silicon oxide (Tang et al. 2015, Wang et al. 2016) and resin (Shi et al. 2016, Shu et al. 2010) etc. Compared with other materials, activated carbon has the advantages of stable chemical properties, large specific surface area, strong adsorption performance and its developed porous structure (Perez-Mayoral et al. 2016). Loaded nZVI has higher stability and resistance to agglomerate than ordinary nZVI, and its stability in water remediation is significantly enhanced.

However, nZVI particles will form an oxide layer on the surface when contacted with air, reducing its reactivity. To solve this problem, the deposition of a second metal (such as Pd, Pt, or Ni) on the surface can significantly enhance the generation of electrons available to reduce contaminants. The nanoparticles may become more stable in the air by inhibiting the oxidation process (Shen et al. 2017, Wang et al. 2013, Zhu et al. 2013). The second metal can also catalyze hydrogenation to promote the removal of pollutants (Rodrigues et al. 2017).

To overcome the shortcomings of nZVI, iron-palladium nanoparticles supported on activated carbon were synthesized by an ultrasonic-assisted electrodeposition method (Costa &Almeida Neto 2020, Tudela et al. 2015). It is expected that the synthesized nZVI/Pd-AC has the physical and chemical properties of the synergistic effect of loading and catalysis, and can be used as a multifunctional material for removing pollutants in water. Therefore, methylene blue (MB), a typical pollutant in printing and dyeing wastewater, was considered as a target pollutant in evaluating the performance of nZVI/Pd-AC. The apparent morphology and microstructure of nZVI/Pd-AC were analyzed by SEM, EDS, XRD and XPS. Various factors affecting the degradation process were investigated, including initial MB concentration, solution pH, solution temperature and other anions. The ability of nZVI-Pd/AC to process MB and its regeneration performance were studied, and GC-MS test results analyzed the removal mechanism and possible degradation path of MB.

2 Materials And Methods

2.1 Materials

Powder activated carbon, acetylene black, polytetrafluoroethylene (PTFE), ferrous sulfate, palladium chloride, saccharin and ammonia were purchased from Aladdin Reagent (Shanghai) Co., Ltd. Absolute ethanol, ammonium chloride, ammonium citrate, sodium dodecyl sulfate, hydrochloric acid, boric acid and methylene blue were obtained from Chron Chemical (Chengdu) Co., Ltd. All these chemicals are analytical reagent and others used are reagent grade. The purity of foamed nickel and iron sheet are both 99.99%. The water used to prepare the aqueous solution is deionized water with a resistivity of 18.2 MΩ.cm.

2.2 Apparatus

An ultrasonic processor (SB-4200 DTS, Ningbo Xinzhi Biotechnology Co., Ltd., China), a magnetic stirrer (DF-101S, Zhengzhou Ketai Laboratory equipment Co., Ltd., China), a pH meter (PHB-4, Shanghai Yidian Co., Ltd., China), an analytical balance (xB6200D, Shanghai Yidian Co., Ltd., China), a DC power supply (KA3005D, Shenzhen Keruiyuan Co., Ltd., China), a vacuum drying oven (DZF-6050, Shanghai Yaoshi Instrument Equipment Factory, China), a field emission scanning electron microscope (SU 8220, Hitachi Co., Japan), an X-ray diffractometer (D8 advance, Bruker Co., Germany), an X-ray photoelectron spectrometer (Escalab 250Xi, Thermo Fisher Co. USA), a spectrophotometer (photolab 7600 UV-VIS, WTW Co., Germany), a ratio surface and porosity analyzer (ASPA-2020, Micromeritics Co., USA) and a gas chromatography-mass spectrometry (GCMS-QP2010, Shimadzu Co., Japan) were used to carry out the experiments.

2.3 Synthesis of nZVI-Pd/AC nanocomposites

In a typical synthesis method(Domenichini et al. 2016, Wang et al. 2015a), 0.075 mol $(NH4)_3C_6H_5O_7$, 0.025 mol $FeSO_4•7H_2O$, 0.225 mol NH_4Cl, 0.001 mol saccharin and 0.0125 g sodium dodecyl sulfate sequentially dissolved into an appropriate amount of ammonia in a 250 mL flask. Then 2.5 mL $PdCl_2$ stock solution (dissolve $PdCl_2$ in 1 mol L^{-1} HCl to make 10 mmol L^{-1} stock solution) and 0.025 mol H_3BO_3 were added.

Added 250 mL deposition solution to a 500 mL sealed electrolytic cell (D = 100mm in diameter and 5cm electrodes spacing), then took it into an ultrasonic generator and started electrodeposition with a DC power supply in nitrogen atmosphere (Fig. 1). The ultrasonic frequency was 40 kHz, power was 260 W, the current density was 3 A, the deposition time is 5min, and the reaction electrode was 40 mm x 40 mm (active area: 30 mm x 40 mm). Activated carbon electrode sheets (powdered activated carbon, acetylene black and PTFE are mixed and pressed in a mass ratio of 8:1:1) and pure iron electrode sheets are used for cathode and anode respectively.

The nZVI/Pd-AC electrode formed by this reaction was washed with deionized water, followed by washing with methanol to prevent immediately rusting. The composite was taken out and dried by vacuum at 60℃ for 2 h.

2.4 Sample characterization

The composite was tested by XRD. Distribution of nZVI and Pd in activated carbon was observed by SEM-EDS. The surface chemistry of nZVI-Pd/AC was analyzed by XPS. The BET surface area analysis of the synthesized nanoparticles was performed by nitrogen adsorption method and surface analyzer.

2.5 Effects of initial concentrations, pH, temperature and NaCl on degradation of MB

To examine the effect of initial concentration on degradation of MB, dye dye solutions were prepared with 20, 30, 40, 50, and 60 mg L^{-1} in deionized water at pH = 5. A 200 mL of dye solution was poured into a 500mL electrolytic tank with nZVI/Pd-AC electrode. The solution was stirred at 100 rpm by magnetic stirring at room temperature. Samples were collected at a preselected time for 3 h. The residual concentrations of dye were quantified by the spectrophotometer at 498 nm for MB. The change in the amount of MB color before and after treatment by nZVI/Pd-AC was quantified by observing the change in the UV/VIS spectrum. The intermediates of MB reduction by nZVI/Pd-AC were analyzed by solid phase micro-extraction (SPME) GC-MS technique. The GC was operated in a temperature programming mode with an initial temperature of 80°C held for 2 min, ramping at 10°C per minute to 150°C, then ramping at 25°C per minute to 280°C and stayed at this temperature for 7 min. The MS conditions were as follows: the ionization mode was electron bombardment (EI), the transmission line temperature was 280°C, the ionization energy was 70 eV, the multiplication voltage was 470 V, the ion source temperature was 230°C, and the solvent was delayed by 3 min.

To optimize the pH of nZVI/Pd-AC treatment for MB contaminated water, the pH was held at 4, 6, 7, 8 and 10, with adjusting by 0.1 mol L^{-1} HCl and 0.1 mol L^{-1} NaOH. MB concentrations were measured in samples at preselected times.

An aqueous phase experiment was conducted to study the effect of reaction temperature to decolorize MB in aqueous solution. A dye solution was prepared in deionized water at an initial concentration of MB of 30 mg L^{-1}. The temperature of the water bath was constant at 25°C, 30°C, 40°C and 50°C, and a piece of nZVI/Pd-AC electrode was added. At room temperature, poured 200 mL dye solution into a 500 mL electrolytic tank, then stirred the solution at 100 rpm. Changes in MB concentrations were measured at preselected times for 3 h.

The actual printing and dyeing wastewater contains a large amount of inorganic salts, such as NaCl. To examine the effect of NaCl to decolorize MB in aqueous, a dye solution was prepared in deionized water at MB of 30 mg L^{-1}. At room temperature, poured 200 mL dye solution into a 500 mL electrolytic tank, with a piece of nZVI/Pd-AC electrode and 0.05%, 0.1% and 0.2% (w/v) NaCl added. The solution was stirred at 100 rpm. Samples were collected at a preselected time for 3 h. The residual concentrations of dye were quantified by spectrophotometer at 498 nm for MB.

2.6 The regeneration process

Take out the nZVI/Pd-AC reacted for 3 hours in the MB solution with concentration of 30 mg L^{-1}, temperature of 25℃ and pH of 5.0, and then rinse the surface deposit solution with pure water. By the method of re-deposition regeneration, the nZVI-Pd/AC was cleaned by ultrasonic processor for 1 min, and then placed it in the electrolytic tank. The deposition solution was the same as the preparation process, in which the current density was 3.0 A and the deposition time was 1 min. Took out the cathode and rinsed with ultrapure water and absolute ethanol 3 times alternately, and then carried out the degradation test.

3 Results And Discussion

3.1 Characterization of the nZVI-Pd/AC

The XRD patterns of the nZVI-AC and nZVI-Pd/AC (Fig. 2) show five characteristic peaks at 44.34°, 51.67°, 76.26°, 92.79° and 98.63°, corresponding to (111), (200), (220), (311) and (222) standard lattice plane of standard Fe^0 samples (JCPDS no. 52–0513), but the peak positions do not precisely match the five characteristic peaks. This may be due to the inclusion of carbon atoms in the grains. According to the Bragg equation, the addition of carbon atoms causes the unit cell to shrink, and these five characteristic peaks move in a larger angle. And no peaks of Pd or other other (hydrogen) oxides are observed in Fig. 2 (a), which may because the energy spectrum of Fe is strong enough to mask the weak signal of Pd. And the surface of the material has very little (hydrogen) oxide deposition, and its content is below the detection limit of XRD (Li et al. 2017a, Wu et al. 2018). As shown in Fig. 2 (b), comparing the XRD patterns of iron-supported and iron-supported palladium, it can be concluded that the peak value of the iron-supported palladium electrode sheet is smaller than that of the iron-supported electrode sheet, which may be due to the reduction of Pd^{2+} by Fe^0 for reducing the crystallinity of Fe^0. Besides, there is not any visible Pd peak on the entire iron-bearing palladium electrode pad. So Pd has a slight lead over the whole electrode sheet with a relatively uniform distribution. On the basis of XRD results, the mean crystal size of nZVI-Pd/AC was calculated by the Scherrer diffraction formula to be 49.82 nm.

The micrograph of activated carbon is shown in Fig. 3 (a). The structural clusters of activated carbon can be observed. The photomicrograph of activated carbon electrode with nZVI is presented in Fig. 3 (b). Compared with the activated carbon, the iron-loaded activated carbon is noticeably smaller, and the particle size distribution is uniform in the range of 40 ~ 80nm. The nanometer nZVI-Pd/AC electrode as Fig. 3 (c), the particle distribution has a uniform, clean-cut, particle size of about 50 nm, and with local agglomeration. According to the multi-point BET method, the BET surface area of the prepared nZVI/Pd nanostructures is 444.43m^2 g^{-1}, which is much larger than the specific surface area of 76.9 m^2 g^{-1} observed by Frost (Frost et al. 2010) et al. This is beneficial to the adsorption and removal of pollutants by nZVI/Pd-AC.

The chemical composition of the prepared activated carbon-supported nZVI/Pd bimetal was determined by EDS analysis (Fig. 4). The molar ratio of Fe to Pd was just 14.9:1, compared with the 1000:1 molar ratio of Fe to Pd in the deposition solution. The palladium content increased markedly, and the reason

may be the existence of a reaction: $Fe^0 + Pd^{2+} = Pd + Fe^{2+}$, which increased the palladium content, and the iron content was reduced compared with the electrode sheet without Pd loading. It is consistent with the XRD results. The 14.9:1 molar ratio of Fe to Pd also confirms the reason for the lack of characteristic peaks of Pd in XRD.

XPS was performed to analyze the chemical composition and oxidation state of representative nZVI-Pd/AC surface species. From the nZVI-Pd/AC wide XPS scan spectrum (Fig. 5 (a)), the Fe 2p, Pd 3d, O 1s and C 1s peaks corresponding to the binding energies of Fe, Pd, O and C were identified respectively. As shown in the Fig. 5 (b), the Fe 2p spectrum deconvolution of nZVI-Pd/AC corresponds to Fe^0 (706.7 eV (Li &Zhang 2006)), Fe2O3 (710.9 eV (Li et al. 2016), 724.5 eV) and FeOOH (713.8 eV). The weak signal displayed at 706.7 eV corresponds to the binding energy of $2P_{3/2}$ of iron, reveals the presence of Fe^0 in the nanoparticles. The Pd 3d spectrum of nZVI-Pd/AC deconvolution has two double peaks. For nZVI-Pd/AC (Fig. 5 (c)), the doublet near 336 eV and 341.3 eV (Li et al. 2018) is attributed to the metal Pd^0, while the other pair near 336.8 eV and 342.4 eV (Shi et al. 2016) is related to the oxidation state Pd (II). Since PdO, Fe_2O_3 and FeOOH have similar characteristic peak positions in this region, there is further investigation of the oxygen state of the scanning O 1s (Fig. 5 (d)). Deconvolution of the O 1s spectrum can be observed four peaks at 529.7 eV, 530.1 eV, 531.1 eV and 531.78 eV, which is commensurate with PdO, Fe_2O_3, FeOOH and H_2O respectively. According to the 2.31:1 ratio of the peak areas of Fe_2O_3 to FeOOH, it can be obtained that the content of Fe_2O_3 is higher than FeOOH, which is consistent with the peak area ratio 2.66:1 collected from the deconvolution of the Fe 2p spectrum. The sample showed the presence of simple substance and oxide while iron and palladium.

3.2 Effect of initial pH of MB degradation

The pH of the solution is important for the reduction of MB by nZVI/Pd-AC. It affects the chemical properties of the solution and the complex surface charge. Previous studies (Xi et al. 2011) reported that the reduction and removal of MB is strongly affected by pH. Figure 6 depicts the effect of different initial pH on the removal of 30 mg L^{-1}MB dye by nZVI/Pd-AC. The results show that the removal effect of MB by nZVI/Pd-AC is better under weakly acidic conditions, and the maximum decomposition efficiency is observed to be 95.76% at pH = 5.0. The removal effect is not good under extremely acidic or alkaline conditions. at pH < 4 or pH > 10, MB removal efficiency is significantly reduced. Under strong acid conditions, excessive H^+ on the surface of the nZVI/Pd-AC electrode sheet will form an electrostatic repulsion with MB, a cationic dye (Hamdy et al. 2018), which prevents the MB from contacting the Fe^0 active site. Under weakly acidic conditions, a small amount of H^+ ions will enhance the corrosion of Fe^0 nanoparticles and promote the generation of hydrogen atoms (Yang &Lee 2005), thereby destroying the chromophore of MB molecules. Under alkaline conditions, with the increase of OH^- concentration, OH^- and Fe^0 form FeOOH, which reduces the active surface sites of the material (Shu et al. 2007), and ultimately leads to a decrease in the decomposition efficiency of MB.

3.3 Effect of the initial concentration of MB

The effect of the initial concentration of MB on the decolorization by nZVI/Pd-AC was studied, as shown in Fig. 7 (a). The initial pH was 5.0 ± 0.5, and the final pH after nZVI/Pd-AC treatment was 6.8 ± 0.5. When the concentration of MB increased from 20 mg L^{-1} to 60 mg L^{-1}, the removal rate increased first and then decreased, and the reaction rate was also highest at the dye concentration of 30 mg L^{-1}. The possible explanation is that a low initial concentration the contact probability of MB molecules with nZVI-Pd/AC is small, causing a slow reaction rate and removal rate, when the concentration is excessive, the surface Fe^0 is covered by the oxide layer, so the MB molecules cannot contact Fe^0 (Fan et al. 2009, Wang et al. 2013). In addition, the high dye concentration will cause competitive adsorption and reduction between dye molecules and nZVI/Pd, and the removal rate will also be reduced.

According to literature reports, the chemical kinetics of vat dyes in solution systems can be described by first-order models or pseudo first-order kinetic model (Lin et al. 2015, Nairat et al. 2015), and is usually modeled by a simple Langmuir-Hinshelwood type rate equation. The model can be described below:

$$\ln \frac{C_t}{C_0} = -k_1 t$$

The k_1 (min^{-1}) is the rate constant of the quasi-first order reaction, and C (mg L^{-1}) is the concentration of MB in the solution. The reaction in the contaminant removal system is a surface-mediated process. If the active surface of Fe^0 is considered unchanged, the reaction can be regarded as quasi-first order kinetics (Bhaumik et al. 2017, Xiong et al. 2007). Table 1 lists the fitted model parameters. The higher R^2 value indicates that the removal of MB is more in line with the pseudo-first-order kinetic modulus. In addition, the degradation rate constant increased with the MB concentration and then decreased, indicating that the reaction rate was not only related to the concentration of pollutants, but also to the active surface site of Fe^0 (Zeng et al. 2017).

Table 1
Pseudo-first-order rate constants k_1 of reductive degradation at various MB concentration

Initial MB concentration (mg L^{-1})	K_1 (min^{-1})	R^2
20	0.0163	0.9907
30	0.0179	0.9706
40	0.0119	0.9734
50	0.0107	0.9771
60	0.0093	0.9779

3.4 Effect of temperature on MB removal

Figure 8 shows the effect of temperature on MB removal. Reacting for 180 min, the MB removal rate increases with increasing temperature. When the solution temperature is 50℃, the MB removal rate reaches a maximum of 98.48%. When the temperature rises from 30℃ to 50℃, the removal efficiency gradually increases. When the temperature changes from 25℃ to 50℃, the removal efficiency in the first 90 min decreases slightly, but it slightly rises finally. The possible reason is the higher temperatures provided more energy for the reaction and accelerated molecule mobility, Which enhanced diffusion and transfer of MB into reactive sites of nZVI/Pd-AC(Zhu et al. 2018). This made MB more accessible to be adsorbed and reduced by nZVI/Pd-AC. Thus, nZVI/Pd-AC achieved higher MB removal efficiency at higher temperatures.

3.5 The effect of NaCl on the removal of MB

Figure 9 shows the effect of NaCl on MB removal. It can be seen that NaCl has a negative effect on the removal of MB. With the increase of NaCl concentration, the removal rate of MB decreases first and then increases, but the increase was not obvious. The removal rate of 0.04 mol L^{-1} NaCl at 180 min was lower than that of 0 mol L^{-1} NaCl. The content of NaCl can hinder the reduction of MB by nZVI-Pd/AC. This may be due to the addition of Cl^-, which inhibits the ionization of MB molecules (Burkinshaw &Salihu 2019b, a), reduces the adsorption of MB on the surface of nZVI/Pd-AC, and thus reduces the reduction and degradation of MB.

3.6 MB removal efficiency of the recycled nZVI-Pd/AC

The reusability/recycling efficiency of catalytic materials is an essential factor in evaluating their cost effectiveness. Figure 10 shows the repeated service life of nZVI-Pd/AC by using 30 mg L^{-1} MB solution with a pH of 5.0 for 3 h of reaction. As the number of reactions increased, its MB removal effect decreased linearly. The MB removal rate was 95.7% in the first batch. In the second and third batches, it decreased to 81.7% and 66.2%, respectively. When the number of consecutive reactions is more than 3, the removal rate was less than 60%.

Due to the poor reusability of the nZVI-Pd/AC material, regeneration experiments were carried out. It's observed that the removal efficiency of the redeposited nZVI-Pd/AC remained at 88% after the fourth reaction. After the fifth regeneration, it decreased by 4.51%, indicating that the prepared nZVI-Pd/AC has a good reproducibility. In the second and third reactions, the MB removal rate increased slightly because new nZVI/Pd nanoparticles were deposited during the redeposition process. The decrease in the MB removal rate after the fifth reaction may be related to the destruction of the composite's pore shape. As a result, the surface area of nZVI-Pd/AC is reduced, lessening the removal rate of MB.

3.7 GC–MS analysis of the MB reductive degradation products

To study the possible degradation path of MB removal by nZVI/Pd-AC, the MB solution after 3 hours of the reaction was used for GC-MS analysis, and the intermediate products produced were characterized in detail. Figure 11 (a) shows the intermediate products of MB decomposition at different m/z. The

fragment ions in the mass spectrum are mostly possible molecular ion peaks. The possible reasons are analyzed: (1) The difference of each intermediate product in the concentration and physical and chemical properties affects its response value in mass spectrometry. (2) In mass spectrometry detection, ion collision may also occur, forming a new ion peak. Combined with the analysis of existing literature (Huang et al. 2010, Zhou et al. 2020), after treatment there are mainly 2-amino-5-dimethylamino-benzenesulfonic acid (m/z = 213) and N,N-dimethylaniline (m/z = 121).

The degradation path of MB dye molecules is speculated from the intermediate products, as shown in Fig. 11 (b). Under the reduction of Fe^0 and the catalytic effect of Pd, MB first breaks the S-C bond and C-N bond to produce intermediate products N,N-dimethylaniline and 2-amino-5-dimethylamino-benzenesulfonic acid. The cleavage of dimethylamino, sulfonic acid, and amino groups eventually degrades into small molecules such as carbon dioxide and water.

4 Conclusions

In this work, nZVI-Pd/AC composites were synthesized via electrodeposition method which was conducted by reducing citrate-complexed Fe^{2+} and ammonia complex Pd^{2+} on the surface of AC cathode. Characterization techniques confirmed the presence of iron and palladium nanoparticles in the samples, and EDS weight percentages of Fe and Pd were 15.84% and 2.06%, respectively. UV-Vis detected the rapid degradation of the dye solution within 180 min, and it conformed to the Langmuir-Hinshelwood pseudo first-order kinetic model. The dye degradation kinetics showed that the reaction occurred at the water-nZVI/Pd interface. Consequent regeneration experiments showed that the nZVI/Pd-GAC composites have a good reusability. Furthermore, the main intermediates including 2-amino-5-dimethylamino-benzenesulfonic acid (m/z = 213) and N,N-dimethylaniline (m/z = 121) were detected by GC–MS. A possible degradation pathway of MB was proposed. The removal mechanism of MB can be concluded as reduction by Fe^0 with enhancement of Pd catalysis.

Declarations

Data Availability

All data generated or analyzed during this study are included in this manuscript.

Acknowledgments

The author acknowledges the Key Laboratory of the Three Gorges Reservoir Region ’ s Eco-Environment for providing all the support during the study period. The author also acknowledges Hongxia Liu for his valuable suggestions and helpful advice on various technical issues examined in this study.

Funding

This research did not receive any specific grant from funding agencies in the public, commercial, or not-for-profit sectors.

Author information

Affiliations

Key Laboratory of the Three Gorges Reservoir Region ' s Eco-Environment (Ministry of Education), Chongqing University,Chongqing, China

Jianjun Liang, Yingtao Long & Yinghao Xue

Chongqing Municipal Design and Research Institute Co., Ltd, Chongqing, China.

Yingtao Long

Contributions

Yingtao Long; Designed and performed experiments, analyzed data, and wrote the manuscript. Jianjun Liang; Supervised the research and edited the paper. Yinghao Xue; Writing - review& editing.

Corresponding author

Correspondence to Jianjun Liang.

Ethics declarations

Competing interests

The authors disclose any actual or potential conflict of interest including any financial, personal, or other relationships with other people or organizations within 3 years of the beginning of the submitted work that could inappropriately influence, or perceived to influence, this work.

Consent to publish

The authors grant the publisher the sole and exclusive license of the full copyright of this contribution.

Ethical approval and consent to participate

All procedures performed in this study were in accordance with the ethical standards of the institutional and/or national research and ethical standards.

References

1. Berge ND, Ramsburg CA (2009): Oil-in-Water Emulsions for Encapsulated Delivery of Reactive Iron Particles. Environmental science & technology 43, 5060-5066

2. Bhaumik M, Maity A, Gupta VK (2017): Synthesis and characterization of Fe0/TiO2 nano-composites for ultrasound assisted enhanced catalytic degradation of reactive black 5 in aqueous solutions. Journal of colloid and interface science 506, 403-414
3. Burkinshaw SM, Salihu G (2019a): The role of auxiliaries in the immersion dyeing of textile fibres: Part 6 analysis of conventional models that describe the manner by which inorganic electrolytes promote reactive dye uptake on cellulosic fibres. Dyes and Pigments 161, 595-604
4. Burkinshaw SM, Salihu G (2019b): The role of auxiliaries in the immersion dyeing of textile fibres part 2: Analysis of conventional models that describe the manner by which inorganic electrolytes promote direct dye uptake on cellulosic fibres. Dyes and Pigments 161, 531-545
5. Chen S-S, Hsu H-D, Li C-W (2005): A new method to produce nanoscale iron for nitrate removal. Journal of Nanoparticle Research 6, 639-647
6. Costa JM, Almeida Neto AFd (2020): Ultrasound-assisted electrodeposition and synthesis of alloys and composite materials: A review. Ultrasonics sonochemistry 68, 105193
7. Domenichini P, Condó AM, Haberkorn N (2016): Structural characterization of FePd nanowires grown by electrodeposition using an acid electrolyte. Materials Chemistry and Physics 177, 164-170
8. Fan J, Guo Y, Wang J, Fan M (2009): Rapid decolorization of azo dye methyl orange in aqueous solution by nanoscale zerovalent iron particles. Journal of Hazardous Materials 166, 904-910
9. Frost RL, Xi Y, He H (2010): Synthesis, characterization of palygorskite supported zero-valent iron and its application for methylene blue adsorption. Journal of colloid and interface science 341, 153-161
10. Fu Y, Peng L, Zeng Q, Yang Y, Song H, Shao J, Liu S, Gu J (2015): High efficient removal of tetracycline from solution by degradation and flocculation with nanoscale zerovalent iron. Chemical Engineering Journal 270, 631-640
11. Hamdy A, Mostafa MK, Nasr M (2018): Zero-valent iron nanoparticles for methylene blue removal from aqueous solutions and textile wastewater treatment, with cost estimation. Water Science and Technology 78, 367-378
12. He F, Zhao D (2007): Manipulating the size and dispersibility of zerovalent iron nanoparticles by use of carboxymethyl cellulose stabilizers. Environmental science & technology 41, 6216-6221
13. Huang FM, Chen L, Wang HL, Yan ZC (2010): Analysis of the degradation mechanism of methylene blue by atmospheric pressure dielectric barrier discharge plasma. Chemical Engineering Journal 162, 250-256
14. Katheresan V, Kansedo J, Lau SY (2018): Efficiency of various recent wastewater dye removal methods: A review. Journal of Environmental Chemical Engineering 6, 4676-4697
15. Li J, Ji Q, Lai B, Yuan D (2017a): Degradation of p-nitrophenol by Fe0/H2O2/persulfate system: Optimization, performance and mechanisms. Journal of the Taiwan Institute of Chemical Engineers 80, 686-694
16. Li J, Wang H, Wang L, Ma C, Luan C, Zhao B, Zhang Z, Zhang H, Cheng X, Liu J (2018): The Preparation of Pd/Foam-Ni Electrode and Its Electrocatalytic Hydrodechlorination for Monochlorophenol Isomers. Catalysts 8

17. Li S, Wang W, Liang F, Zhang WX (2017b): Heavy metal removal using nanoscale zero-valent iron (nZVI): Theory and application. J Hazard Mater 322, 163-171
18. Li X-q, Zhang W-x (2006): Iron Nanoparticles: the Core–Shell Structure and Unique Properties for Ni(II) Sequestration. Langmuir 22, 4638-4642
19. Li Y, Li X, Xiao Y, Wei C, Han D, Huang W (2016): Catalytic debromination of tetrabromobisphenol A by Ni/nZVI bimetallic particles. Chemical Engineering Journal 284, 1242-1250
20. Lin J, Weng X, Jin X, Megharaj M, Naidu R, Chen Z (2015): Reactivity of iron-based nanoparticles by green synthesis under various atmospheres and their removal mechanism of methylene blue. RSC Advances 5, 70874-70882
21. Liu J, Liu A, Zhang W-x (2016): The influence of polyelectrolyte modification on nanoscale zero-valent iron (nZVI): Aggregation, sedimentation, and reactivity with Ni(II) in water. Chemical Engineering Journal 303, 268-274
22. Nairat M, Shahwan T, Eroğlu AE, Fuchs H (2015): Incorporation of iron nanoparticles into clinoptilolite and its application for the removal of cationic and anionic dyes. Journal of Industrial and Engineering Chemistry 21, 1143-1151
23. Perez-Mayoral E, Calvino-Casilda V, Soriano E (2016): Metal-supported carbon-based materials: opportunities and challenges in the synthesis of valuable products. Catal. Sci. Technol. 6, 1265-1291
24. Qian LB, Zhang WY, Yan JC, Han L, Chen Y, Ouyang D, Chen MF (2017): Nanoscale zero-valent iron supported by biochars produced at different temperatures: Synthesis mechanism and effect on Cr(VI) removal. Environmental Pollution 223, 153-160
25. Rajeswari A, Christy EJS, Mary GIC, Jayaraj K, Pius A (2019): Cellulose acetate based biopolymeric mixed matrix membranes with various nanoparticles for environmental remediation-A comparative study. Journal of Environmental Chemical Engineering 7
26. Rodrigues R, Betelu S, Colombano S, Masselot G, Tzedakis T, Ignatiadis I (2017): Reductive Dechlorination of Hexachlorobutadiene by a Pd/Fe Microparticle Suspension in Dissolved Lactic Acid Polymers: Degradation Mechanism and Kinetics. Industrial & Engineering Chemistry Research 56, 12092-12100
27. Satapanajaru T, Chompuchan C, Suntornchot P, Pengthamkeerati P (2011): Enhancing decolorization of Reactive Black 5 and Reactive Red 198 during nano zerovalent iron treatment. Desalination 266, 218-230
28. Shen W, Mu Y, Wang B, Ai Z, Zhang L (2017): Enhanced aerobic degradation of 4-chlorophenol with iron-nickel nanoparticles. Applied Surface Science 393, 316-324
29. Shi J, Long C, Li A (2016): Selective reduction of nitrate into nitrogen using Fe–Pd bimetallic nanoparticle supported on chelating resin at near-neutral pH. Chemical Engineering Journal 286, 408-415
30. Shu H-Y, Chang M-C, Yu H-H, Chen W-H (2007): Reduction of an azo dye Acid Black 24 solution using synthesized nanoscale zerovalent iron particles. Journal of colloid and interface science 314, 89-97

31. Shu HY, Chang MC, Chen CC, Chen PE (2010): Using resin supported nano zero-valent iron particles for decoloration of Acid Blue 113 azo dye solution. J Hazard Mater 184, 499-505
32. Tang L, Tang J, Zeng G, Yang G, Xie X, Zhou Y, Pang Y, Fang Y, Wang J, Xiong W (2015): Rapid reductive degradation of aqueous p-nitrophenol using nanoscale zero-valent iron particles immobilized on mesoporous silica with enhanced antioxidation effect. Applied Surface Science 333, 220-228
33. Tian H, Liang Y, Zhu T, Zeng X, Sun Y (2018): Surfactant-enhanced PEG-4000-NZVI for remediating trichloroethylene-contaminated soil. Chemosphere 195, 585-593
34. Tudela I, Zhang Y, Pal M, Kerr I, Mason TJ, Cobley AJ (2015): Ultrasound-assisted electrodeposition of nickel: Effect of ultrasonic power on the characteristics of thin coatings. Surf. Coat. Technol. 264, 49-59
35. Verma AK, Dash RR, Bhunia P (2012): A review on chemical coagulation/flocculation technologies for removal of colour from textile wastewaters. Journal of environmental management 93, 154-168
36. Wang C, Liu T, Bu F, Liu H (2015a): Perchlorate Removal Using a Minimized Dosage of Electrodeposited Zero-Valent Iron. J. Environ. Eng.-ASCE 141, 04014064
37. Wang C, Liu TF, Bu F, Liu H (2015b): Perchlorate Removal Using a Minimized Dosage of Electrodeposited Zero-Valent Iron. J. Environ. Eng.-ASCE 141, 6
38. Wang P, Wang X, Yu S, Zou Y, Wang J, Chen Z, Alharbi NS, Alsaedi A, Hayat T, Chen Y, Wang X (2016): Silica coated Fe 3 O 4 magnetic nanospheres for high removal of organic pollutants from wastewater. Chemical Engineering Journal 306, 280-288
39. Wang T, Su J, Jin X, Chen Z, Megharaj M, Naidu R (2013): Functional clay supported bimetallic nZVI/Pd nanoparticles used for removal of methyl orange from aqueous solution. Journal of Hazardous Materials 262, 819-825
40. Wang X, Wang P, Ma J, Liu H, Ning P (2015c): Synthesis, characterization, and reactivity of cellulose modified nano zero-valent iron for dye discoloration. Applied Surface Science 345, 57-66
41. Wu J, Yi Y, Li Y, Fang Z, Tsang EP (2016): Excellently reactive Ni/Fe bimetallic catalyst supported by biochar for the remediation of decabromodiphenyl contaminated soil: Reactivity, mechanism, pathways and reducing secondary risks. J Hazard Mater 320, 341-349
42. Wu Y, Yue Q, Gao Y, Ren Z, Gao B (2018): Performance of bimetallic nanoscale zero-valent iron particles for removal of oxytetracycline. Journal of Environmental Sciences 69, 173-182
43. Xi Y, Megharaj M, Naidu R (2011): Dispersion of zerovalent iron nanoparticles onto bentonites and use of these catalysts for orange II decolourisation. Applied Clay Science 53, 716-722
44. Xiong Z, Zhao D, Pan G (2007): Rapid and complete destruction of perchlorate in water and ion-exchange brine using stabilized zero-valent iron nanoparticles. Water research 41, 3497-3505
45. Xue YH, Xiang P, Wang HW, Long YT, Lian HL, Shi WX (2019): Mechanistic insights into selective adsorption and separation of multi-component anionic dyes using magnetic zeolite imidazolate framework-67 composites. Journal of Molecular Liquids 296

46. Yan W, Lien H-L, Koel BE, Zhang W-x (2013): Iron nanoparticles for environmental clean-up: recent developments and future outlook. Environ. Sci.: Processes Impacts 15, 63-77
47. Yang B, Tian Z, Zhang L, Guo Y, Yan S (2015): Enhanced heterogeneous Fenton degradation of Methylene Blue by nanoscale zero valent iron (nZVI) assembled on magnetic Fe3O4/reduced graphene oxide. Journal of Water Process Engineering 5, 101-111
48. Yang GCC, Lee H-L (2005): Chemical reduction of nitrate by nanosized iron: kinetics and pathways. Water research 39, 884-894
49. Zeng Y, Walker H, Zhu Q (2017): Reduction of nitrate by NaY zeolite supported Fe, Cu/Fe and Mn/Fe nanoparticles. Journal of Hazardous Materials 324, 605-616
50. Zhang X, Lin Y-m, Chen Z-l (2009): 2,4,6-Trinitrotoluene reduction kinetics in aqueous solution using nanoscale zero-valent iron. Journal of Hazardous Materials 165, 923-927
51. Zhao R, Wang Y, Li X, Sun B, Wang C (2015): Synthesis of beta-Cyclodextrin-Based Electrospun Nanofiber Membranes for Highly Efficient Adsorption and Separation of Methylene Blue. Acs Applied Materials & Interfaces 7, 26649-26657
52. Zhou Y, Li Z, Hao C, Zhang Y, Chai S, Han G, Xu H, Lu J, Dang Y, Sun X, Fu Y (2020): Electrocatalysis enhancement of α, β-PbO2 nanocrystals induced via rare earth Er(III) doping strategy: Principle, degradation application and electrocatalytic mechanism. Electrochimica Acta 333, 135535
53. Zhu F, Ma S, Liu T, Deng X (2018): Green synthesis of nano zero-valent iron/Cu by green tea to remove hexavalent chromium from groundwater. Journal of Cleaner Production 174, 184-190
54. Zhu K, Sun C, Chen H, Baig SA, Sheng T, Xu X (2013): Enhanced catalytic hydrodechlorination of 2,4-dichlorophenoxyacetic acid by nanoscale zero valent iron with electrochemical technique using a palladium/nickel foam electrode. Chemical Engineering Journal 223, 192-199

Figures

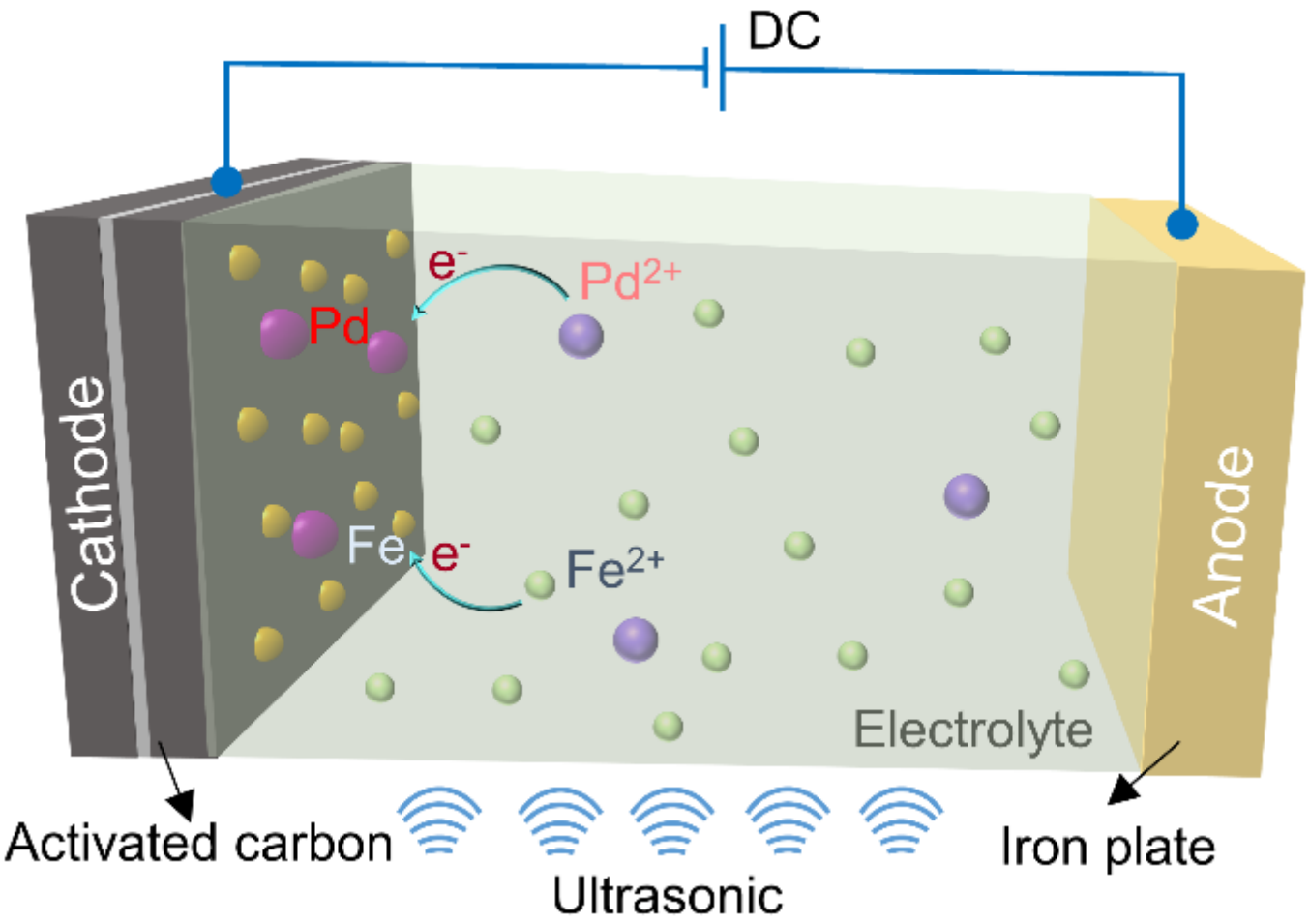

Figure 1

Schematic illustration of the electrodeposition method under the action of ultrasonic.

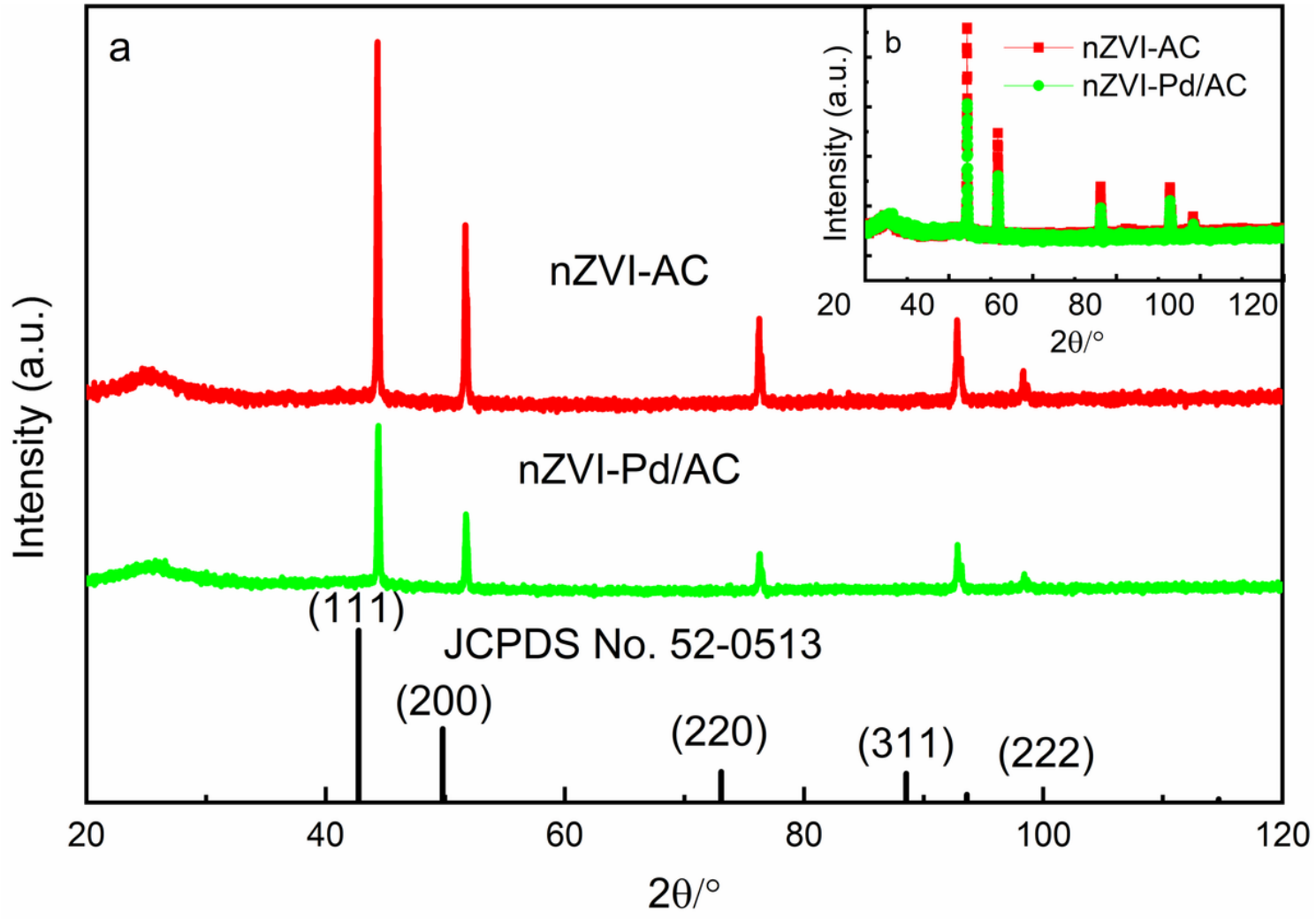

Figure 2

XRD pattern of bimetallic nanoscale nZVI/Pd particles.

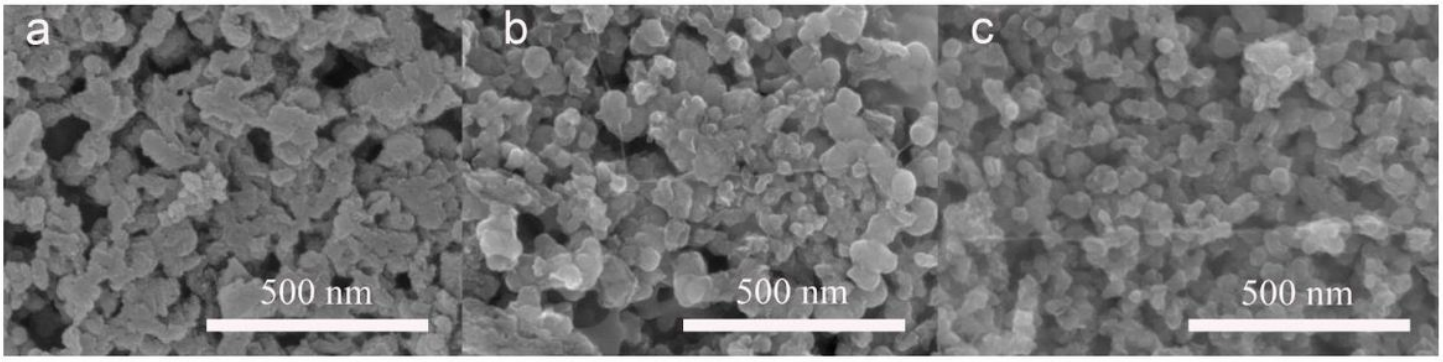

Figure 3

SEM images of AC (a), nZVI-AC (b) and nZVI-Pd/AC (c).

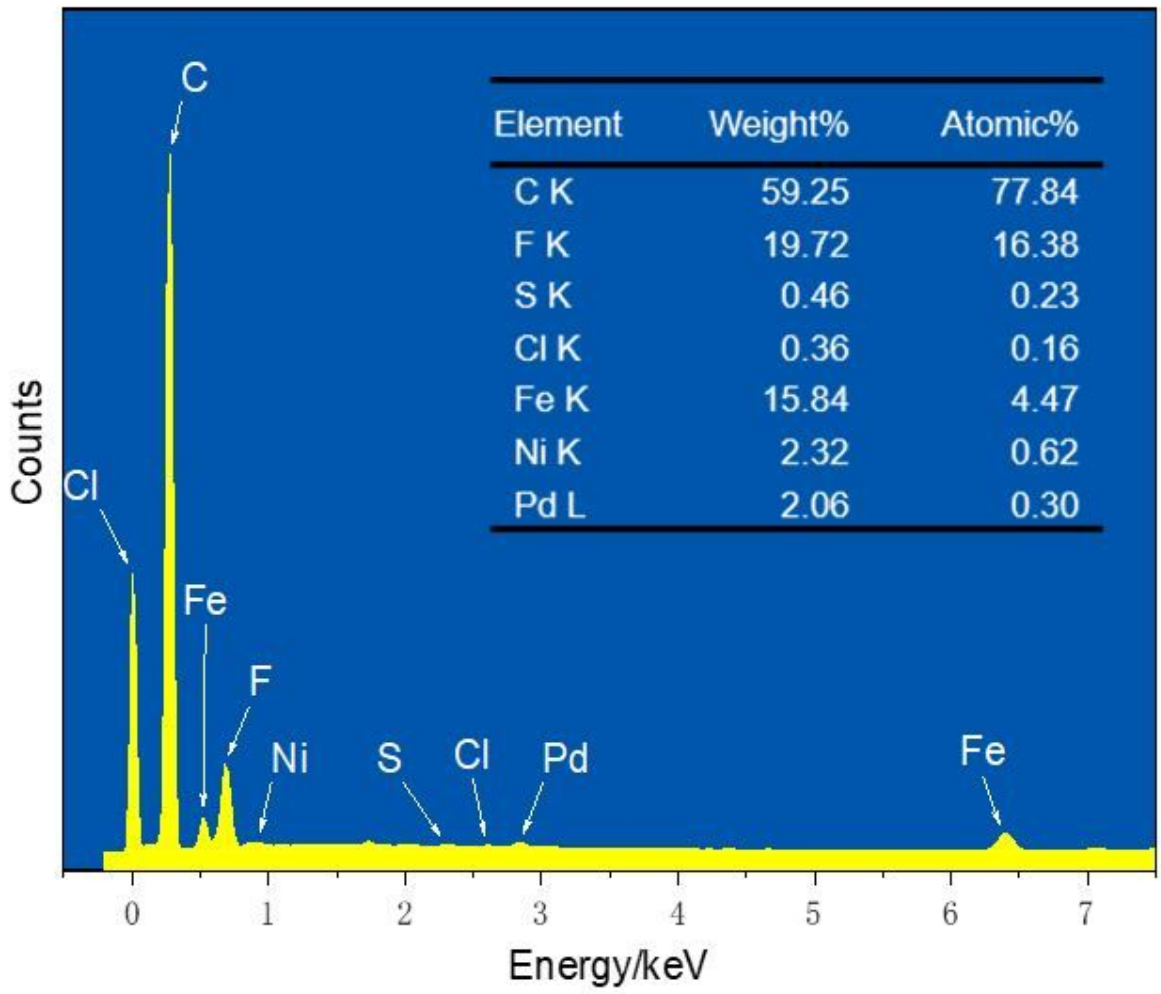

Figure 4

EDS spectrum of activated carbon-supported iron-palladium.

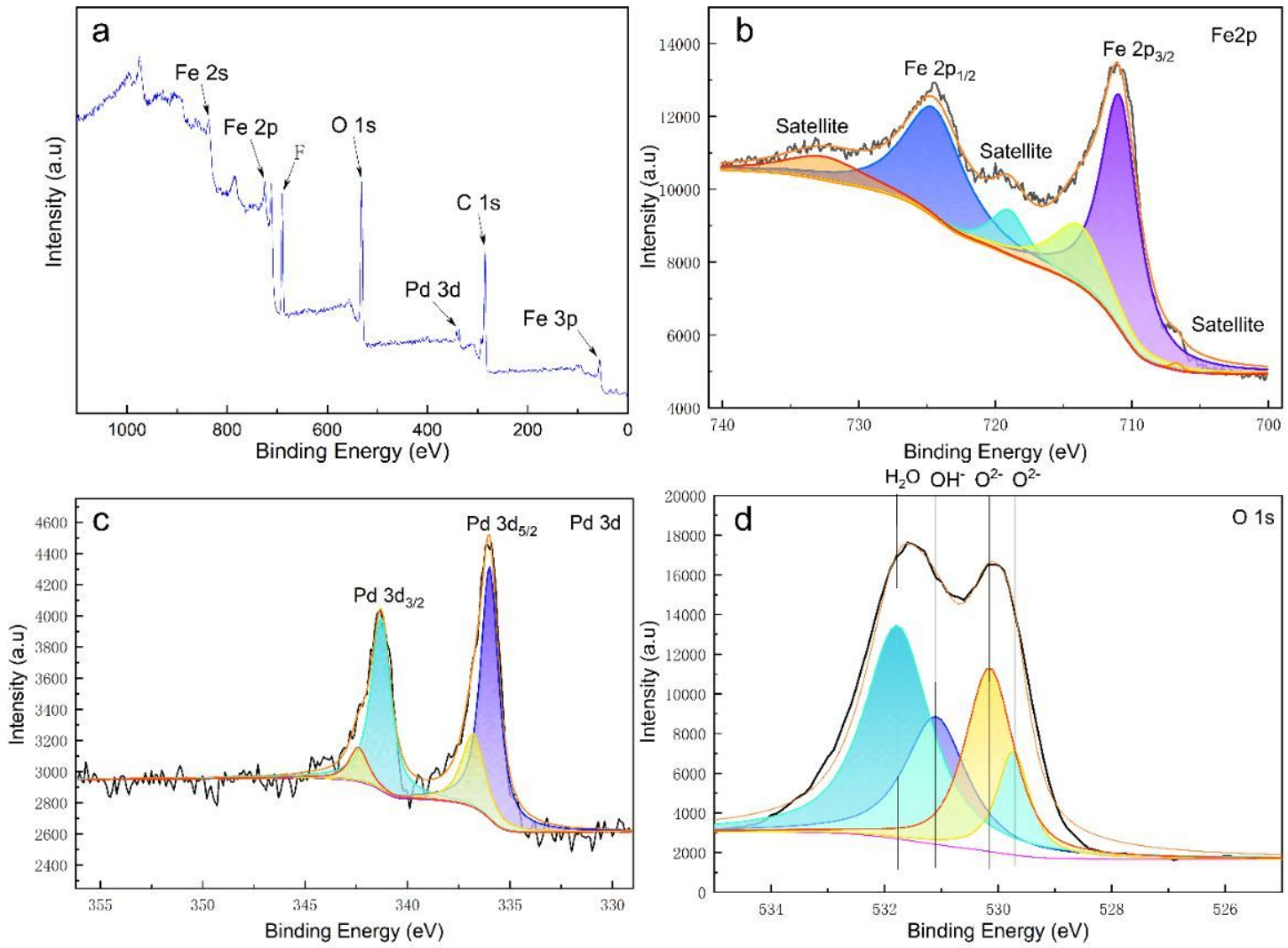

Figure 5

XPS survey spectrum of nZVI-Pd/AC (a) and high-resolution peaks of Fe 2p (b), Pd 3d (c) and O 1s (d) region.

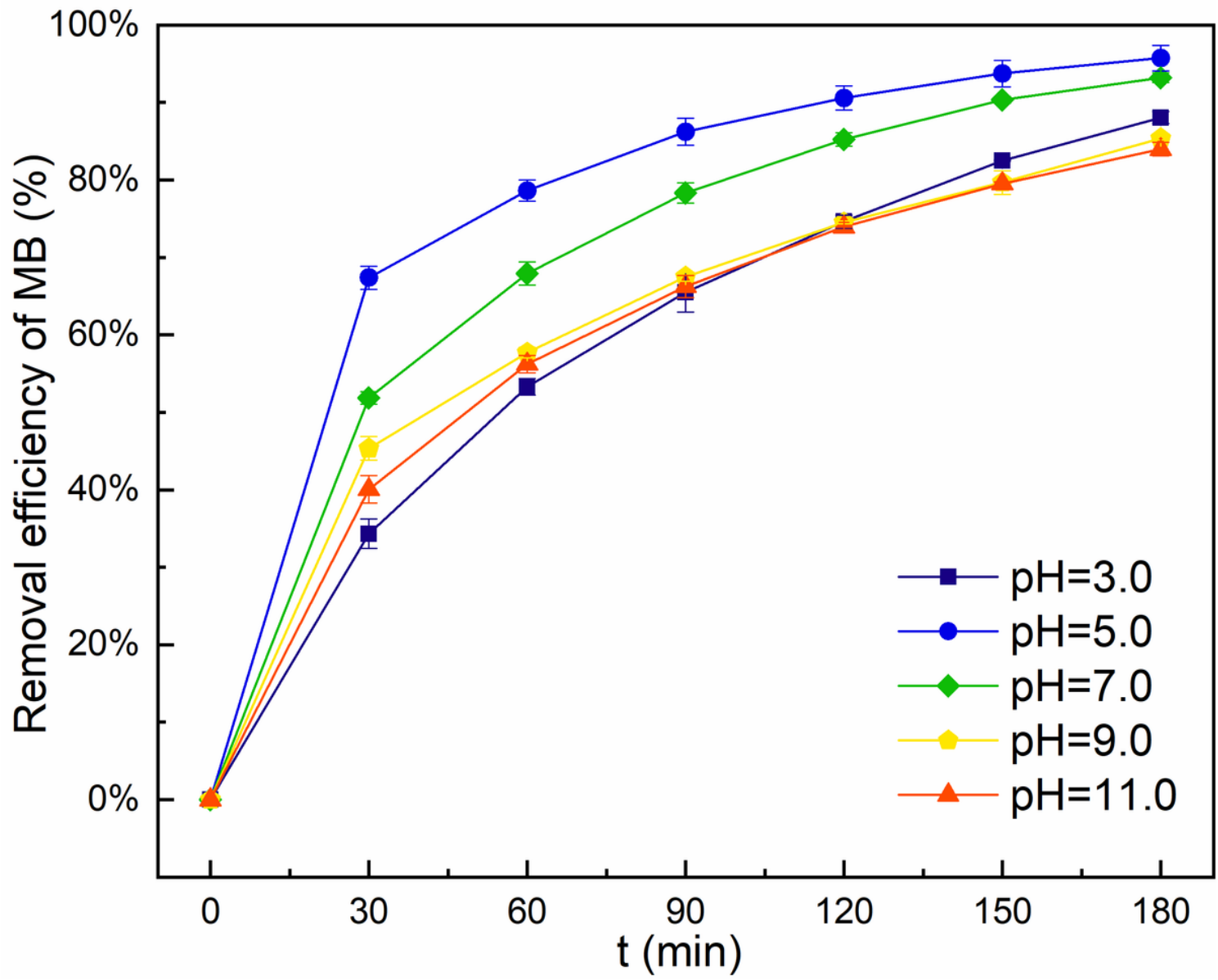

Figure 6

Effect of the initial pH on percent removal of MB dye concentration. Initial conditions: MB concentration 30 mg L-1, temperature 25°C, reactor volume 0.25 L, and reaction 3 h.

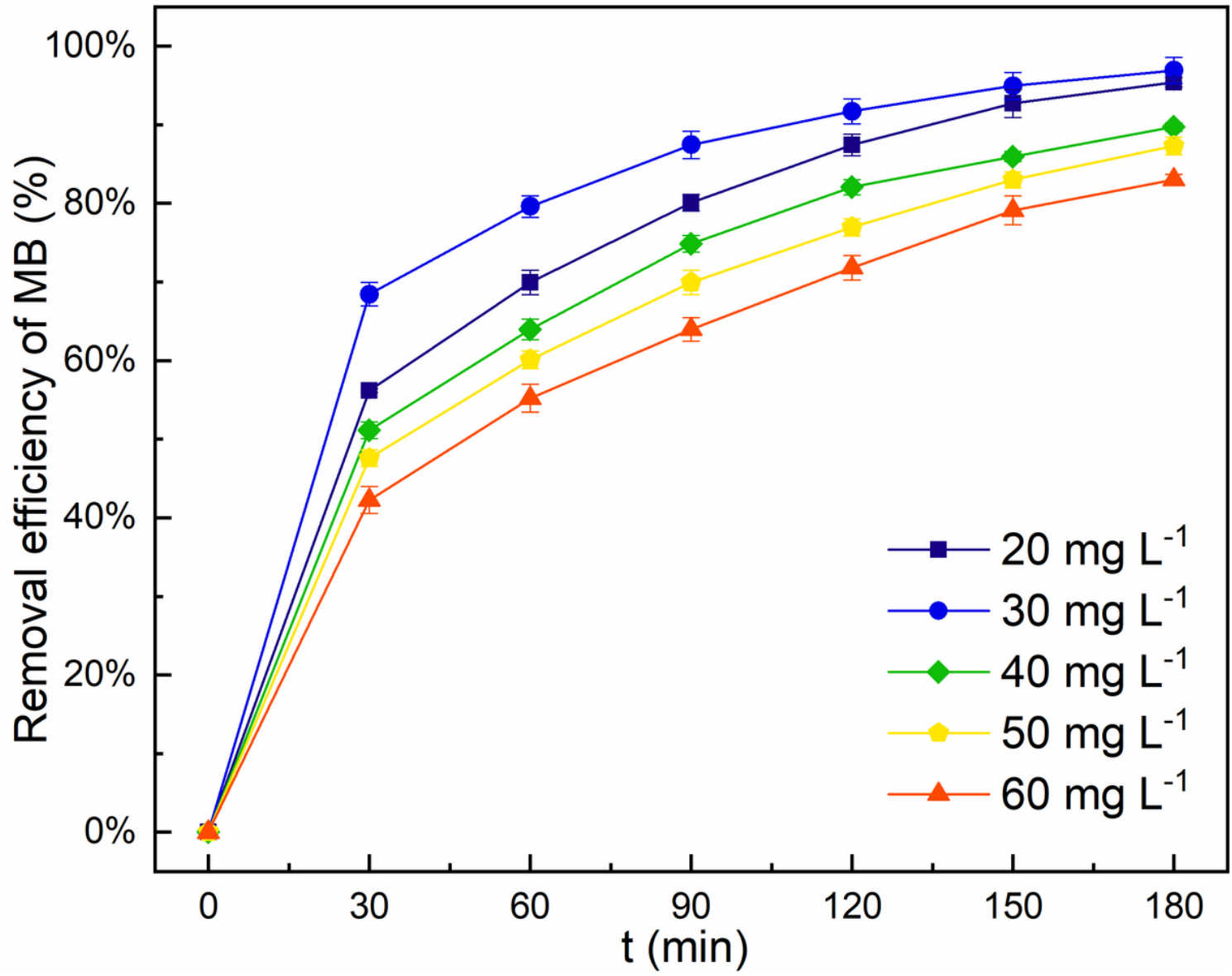

Figure 7

Effect of initial concentration on MB removal efficiency by nZVI-Pd/AC. Initial conditions: pH=5.0, temperture 25℃, reactor volume 0.25 L, and reaction 3 h,.

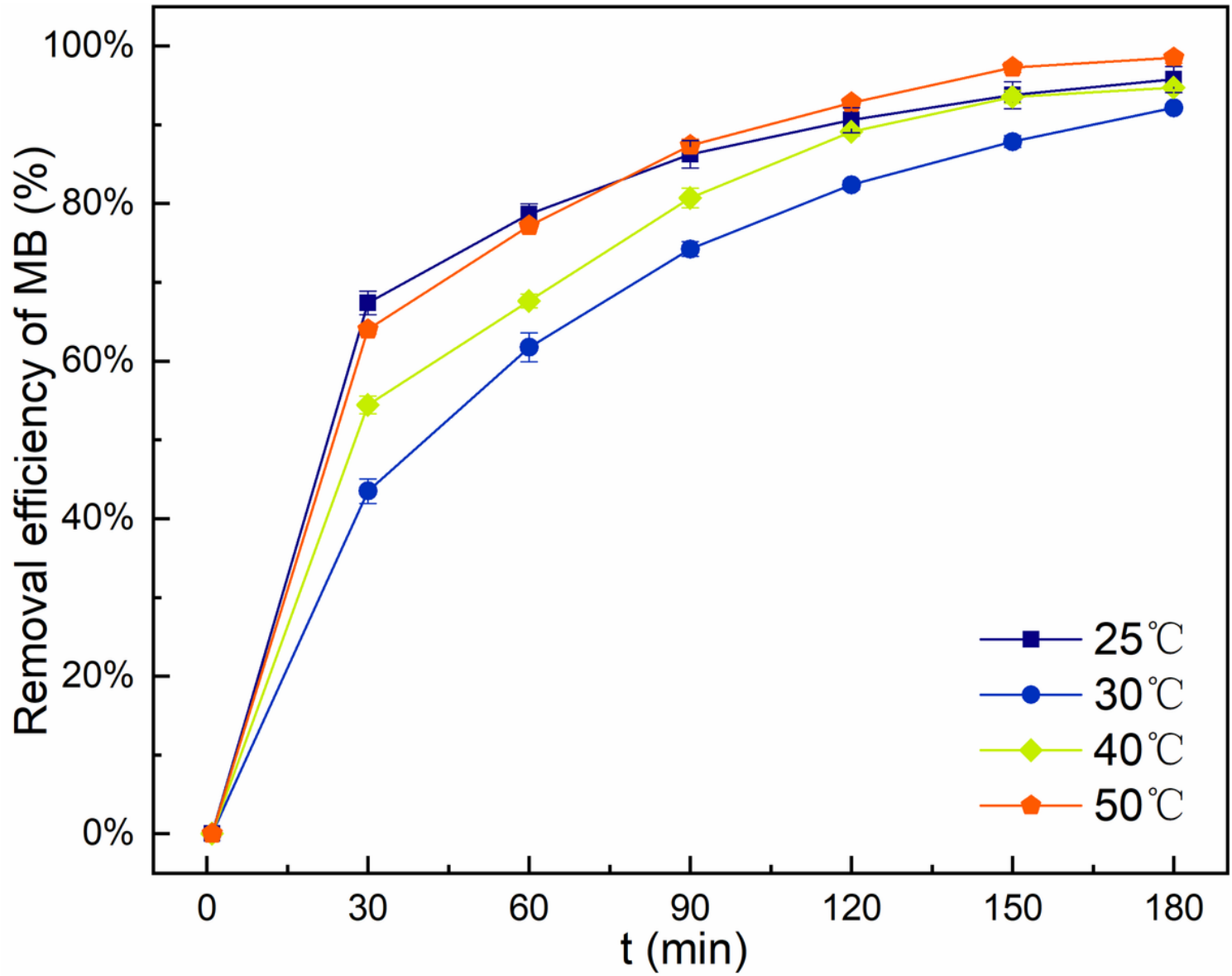

Figure 8

Effect of temperature on MB removal efficiency. Initial conditions: pH=5.0, temperture 25℃, reaction 3 h, reactor volume 0.25 L, and initial MB concentration 30 mg L-1.

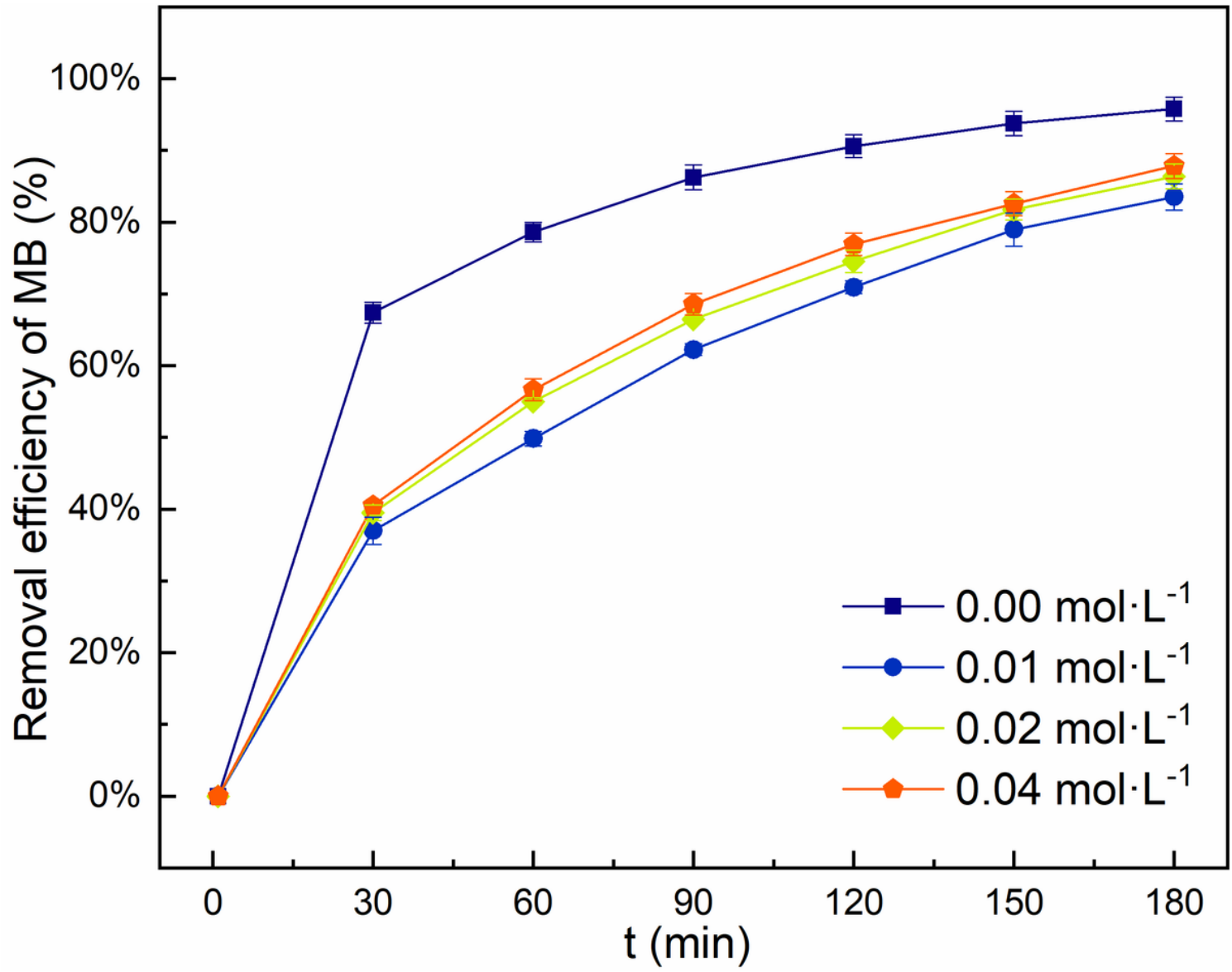

Figure 9

Effect of NaCl on MB removal efficiency. Initial conditions: pH=5.0, temperture 25°C, reaction 3 h, reactor volume 0.25 L, and initial MB concentration 30 mg L-1.

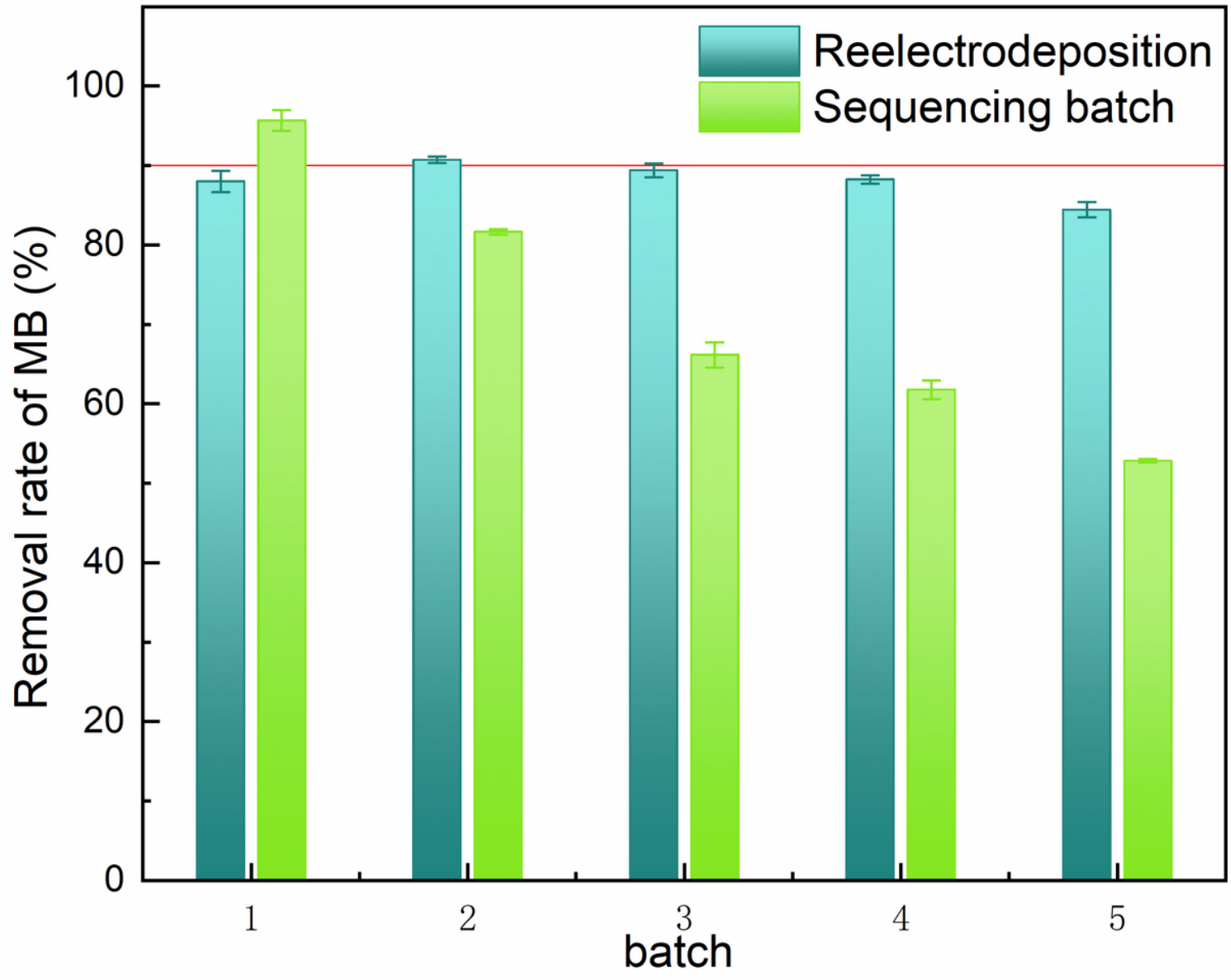

Figure 10

nZVI-Pd/AC reusability and regeneration. Initial conditions: pH=5.0, temperture 25°C, reaction 3 h, reactor volume 0.25 L, and initial MB concentration 30 mg L-1.

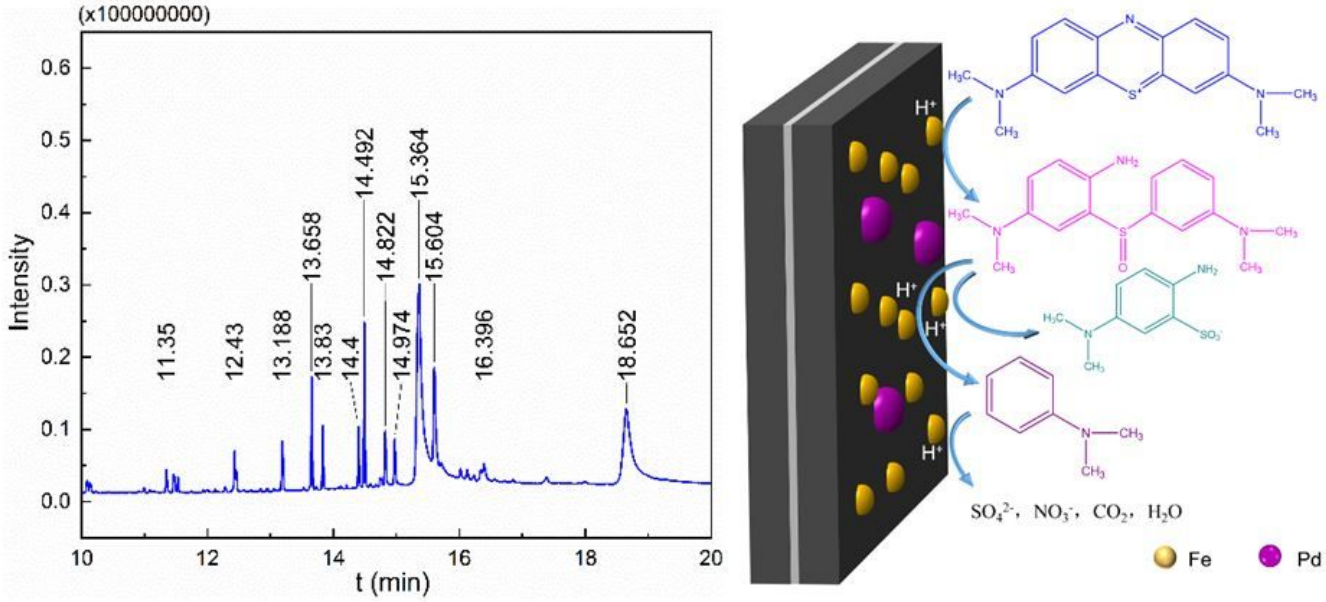

Figure 11

The mass spectrum of MB solution degraded for 3 h (a) and the MB degradation path analysis (b).

Supplementary Files

This is a list of supplementary files associated with this preprint. Click to download.

- GraphicalAbstract.jpg